Self-mixing in multi-transverse mode semiconductor lasers: model and potential application to multi-parametric sensing

L. Columbo,[1,2,*] **M. Brambilla,**[1] **M. Dabbicco,**[1] **and G. Scamarcio**[1]

[1]*CNR-Istituto di Fotonica e Nanotecnologie UOS Bari, c/o Dipartimento di Fisica Interateneo, Via Amendola 173, 70126 Bari, Italy*

[2]*Dipartimento di Fisica e Matematica, Universitá degli studi dell'Insubria, Via Valleggio 11, 22100 Como, Italy*

[*]*lorenzo.columbo@fisica.uniba.it*

Abstract: A general model is proposed for a Vertical Cavity Surface Emitting Laser (VCSEL) with medium aspect ratio whose field profile can be described by a limited set of Gauss-Laguerre modes. The model is adapted to self-mixing schemes by supposing that the output beam is reinjected into the laser cavity by an external target mirror. We show that the self-mixing interferometric signal exhibits features peculiar of the spatial distribution of the emitted field and the target-reflected field and we suggest an applicative scheme that could be exploited for experimental displacement measurements. In particular, regimes of transverse mode-locking are found, where we propose an operational scheme for a sensor that can be used to simultaneously measure independent components of the target displacement like target translations along the optical axis (longitudinal axis) and target rotations in a plane orthogonal to the optical axis (transverse plane).

OCIS codes: (140.5960) Semiconductor lasers; (190.4420) Nonlinear optics, transverse effects in; (280.3420) Laser sensors; (280.4788) Optical sensing and sensors; (120.3180) Interferometry; (120.3930) Metrological instrumentation.

References and links

1. D. M. Kane and K. A. Shore, *Unlocking Dynamical Diversity. Optical Feedback Effects on Semiconductor Lasers* (John Wiley and Sons, 2005).
2. S. Donati, G. Giuliani, and S. Merlo, "Laser diode feedback inteferometer for measurement of displacements without ambiguity," IEEE J. Quantum Electron. **31**, 113–119 (1995).
3. S. Ottonelli, M. Dabbicco, F. De Lucia, and G. Scamarcio, "Simultaneous measurement of linear and transverse displacements by laser self-mixing," Appl. Opt. **48**, 1784-1789 (2009).
4. J. R. Tucker, J. L. Baque, Y. L. Lim, A. V. Zvyagin, A. D. Rakic, "Parallel self-mixing imaging system based on an array of vertical-cavity surface-emitting lasers," Appl. Opt. **46**, 6237–6246 (2007).
5. Y. L. Lim, M. Nikolic, K. Bertling, R. Kliese, and A. D. Rakic, "Self-mixing imaging sensor using a monolithic VCSEL array with parallel readout," Opt. Express **17**, 5517–5525 (2009).
6. Y. L. Lim, R. Kliese, K. Bertling, K. Tanimizu, P. A. Jacobs, and A. D. Rakic, "Self-mixing flow sensor using a monolithic VCSEL array with parallel readout," Opt. Express **18**, 11720–11727 (2010).
7. "Z. Liu, D. Lin, H. Jiang, and C. Yin, "Roll angle interferometer by means of wave plates," Sens. Actuators, A **104**, 127–131 (2003).
8. C-M. Wu and Y-T. Chuang, "Roll angular displacement measurement system with microradian accuracy," Sens. Actuators, A **116**, 145–149 (2004).

#156317 - $15.00 USD Received 11 Oct 2011; revised 9 Dec 2011; accepted 2 Jan 2012; published 5 Mar 2012

9. W. S. Park and H. S. Cho, "Measurement of fine 6-degrees-of-freedom displacement of rigid bodies through splitting a laser beam: experimental investigation," Opt. Eng. **41**, 860–871 (2002).
10. C. J. Chen, P. D. Lin, and W. Y. Jywe, "An optoelectronic measurement system for measuring 6-degree-of-freedom motion error of rotary parts," Opt. Express **15**, 14601–14617 (2007).
11. S. Ottonelli, M. Dabbicco, F. De Lucia, M. di Vietro, and G. Scamarcio, "Laser-self-mixing interferometry for mechatronics applications," Sensors **9**, 3527–3548 (2009).
12. F. P. Mezzapesa, L. Columbo, M. Brambilla, M. Dabbicco, A. Ancona, T. Sibillano, F. De Lucia, P. M. Lugará, and G. Scamarcio, "Simultaneous measurement of multiple target displacements by self-mixing interferometry in a single laser diode," Opt. Express **19**, 16160–16173 (2011).
13. C. J. Chang-Hasnain, M. Orenstein, A. Von Lehmen, l. T. Florez, J. P. Harbison, and N. G. Stoffel, "Transverse mode characteristics of vertical cavity surface-emitting lasers," Appl. Phys. Lett. **57**, 218–220 (1990).
14. H. Lia, T. L. Lucas, J. G. McInerney, and R. A. Morgan, "Transverse modes and patterns of electrically pumped vertical-cavity surface-emitting semiconductor lasers," Chaos, Solitons Fractals **4**, 1619–1636 (1994).
15. J. U. Nöckel, G. Bourdon, E. Le Ru, R. Adams, I. Robert, J.-M. Moison, and I. Abram, "Mode structure and ray dynamics of a parabolic dome microcavity," Phys. Rev. E **62**, 8677–8699 (2000).
16. S.-H. Park, Y. Park, H. Kim, H. Jeon, S. M. Hwang, J. K. Lee, S. H. Nam, B. C. Koh, J. Y. Sohn, and D. S. Kim, "Microlensed vertical-cavity surface-emitting laser for stable single fundamental mode operation," Appl. Phys. Lett. **80**, 183–185 (2002).
17. M. T. Cha and R. Gordon, "Spatially Filtered Feedback for Mode Control in Vertical-Cavity Surface-Emitting Lasers," J. Lightwave Technol. **26**, 3893–3900 (2008).
18. F. Prati, A. Tesei, L. A. Lugiato, and R.J. Horowicz, "Stable states in surface-emitting semiconductor lasers," Chaos, Solitons Fractals **4**, 1637–1654 (1994).
19. A. Valle, J. Sarma, and K. A. Shore, "Dynamics of transverse mode competition in vertical cavity surface emitting laser diodes," Opt. Commun. **115**, 297–302 (1995).
20. L. A. Lugiato, "Spatio-temporal structures. Part I," Phys. Rep. **219**, 293–310 (1992).
21. F. Prati, M. Travagnin, and L. A. Lugiato, "Logic gates and optical switching with vertical-cavity surface-emitting lasers," Phys. Rev. A **55**, 690–700 (1997).
22. M. San Miguel, Q. Feng, and J. V. Moloney, "Light-polarization dynamics in surface-emitting semiconductor lasers," Phys. Rev. A **52**, 1728–1739 (1995).
23. F. Prati, G. Tissoni, M. San Miguel, and N. B Abraham, "Vector vortices and polarization state of low-order transverse modes in a VCSEL," Opt. Commun. **143**, 133–146 (1997).
24. J Martń-Regalado, S. Balle, M. San Miguel, A. Valle and L. Pesquera, "Polarization and transverse-mode selection in quantum-well vertical-cavity surface-emitting lasers: index- and gain-guided devices," Quantum Semiclassic. Opt. **9**, 713–736 (1997).
25. R. Lang and K. Kobayashi, "External optical feedback effects on semiconductor injection laser proprieties," IEEE J. Quantum Electron. **16**, 347–355 (1980).
26. J. Y. Law and G. P. Agrawal, "Effects of optical feedback on static and dynamic characteristics of vertical-cavity surface-emitting lasers," IEEE J. Sel. Top. Quantum Electron. **3**, 353-3-58 (1997).
27. M. S. Torre, C. Masoller, and P. Mandel, "Transverse mode dynamics in vertical-cavity surface-emitting lasers with optical feedback," Phys. Rev. A **66**, 053817 (2002).
28. K. Green, B. Krauskopf, and D. Lenstra, "External cavity mode structure of a two-mode VCSEL subject to optical feedback," Opt. Commun. **277**, 359–371 (2007).
29. G. Oppo and G. Dalessandro, "Gauss–Laguerre modes - a sensible basis for laser dynamics," Opt. Commun. **88** , 130–136 (1992).
30. L. A. Lugiato, F. Prati, L. M. Narducci, P. Ru, J. R. Tredicce, and D. K. Bandy, "Role of transverse effects in laser instabilities," Phys. Rev. A **37**, 3847–3866 (1988).
31. M. Brambilla, M. Cattaneo, L. A. Lugiato, R. Pirovano, F. Prati, A. J. Kent, G.-L. Oppo, A. B. Coates, C. O. Weiss, C. Green, E. J. DAngelo, and J. R. Tredicce, "Dynamical transverse laser patterns. I. Theory," Phys. Rev. A **49**, 1427–1451 (1994).
32. A. B. Coates, C. O. Weiss, C. Green, E. J. DAngelo, J. R. Tredicce, M. Brambilla, M. Cattaneo, L. A. Lugiato, R. Pirovano, F. Prati, A. J. Kent, and G.-L. Oppo, "Dynamical transverse laser patterns. II. Experiments," Phys. Rev. A **49**, 1452–1466(1994).
33. F. Prati, M. Brambilla, and L. A. Lugiato, "Pattern formation in lasers," Riv. Nuovo Cimento **17**, 1–85 (1994).
34. S. Barland, J. R. Tredicce, M. Brambilla, L. A. Lugiato, S. Balle, M. Giudici, T. Maggipinto, L. Spinelli, G. Tissoni, T. Kndl, M. Miller, and R. Jger, "Cavity solitons as pixels in semiconductor microcavities," Nature **419**, 699–702 (2002).
35. C. O. Weiss, H. R. Telle, K. Staliunas, and M. Brambilla, "Restless optical vortex," Phys. Rev. A **47**, R1616–R1619 (1993).
36. E. K. Lau, X. Zhao, H.-K. Sung, D. Parekh, C. Chang-Hasnain, and M. C. Wu, "Strong optical injection-locked semiconductor lasers demonstrating $> 100-GHz$ resonance frequencies and $80-GHz$ intrinsic bandwidths," Opt. Express **16**, 6609–6618 (2008).
37. G Slekys, I Ganne, I Sagnes and R Kuszelewicz, "Optical pattern formation in passive semiconductor microres-

#156317 - $15.00 USD Received 11 Oct 2011; revised 9 Dec 2011; accepted 2 Jan 2012; published 5 Mar 2012

onators," J. Opt. B: Quantum Semiclassical Opt. **2**, 443–446 (2000).
38. A. C. Tropper, H. D. Foreman, A. Garnache, K. G. Wilcox, and S. H. Hoogland, "Vertical-external-cavity semiconductor lasers," J. Phys. D: Appl. Phys. **37**, R75–R85 (2004).
39. D. Guo, M. Wang, and S. Tan, "Self-mixing interferometer based on sinusoidal phase modulating technique," Opt. Express **13**, 1537–1543 (2005).
40. F. A. Chollet, G. M. Hegde, A .K. Asundi, and A. Q. Liu, "Simple extra-short external cavity laser self-mixing interferometer for acceleration sensing," Proc. SPIE **4596**, 272–279 (2001).
41. G. Giuliani, S. Donati, M. Passerini, and T. Bosch, "Angle measurement by injection detection in a laser diode," Opt. Eng. **40**, 95–99 (2001).
42. S. Wolff and H. Fouckhardt, "Intracavity stabilization of broad area lasers by structured delayed optical feedback," Opt. Express **7**, 222–227 (2000).
43. A. E. Siegman, *Lasers* (University Science Books, 1986).

1. Introduction

The self-mixing interferometry in semiconductor lasers has been largely exploited in the field of high precision metrology to realize compact, contactless, sensors for real time measurements of absolute distance, vibrations, rotations, flow rate [1, 2].

When the laser source is a conventional diode laser emitting on the Gaussian mode, the quantity that is directly related to the measure of target displacements is the laser intensity. The latter, in presence of optical feedback provided by the target, is periodically modulated at half the wavelength; so that the number of the interference fringes in the signal visualized by a digital oscilloscope connected to the laser integrated photodiode provides a measure of the target displacements. Moreover, there exist certain feedback regimes where the interferometric signal has an asymmetric sawtooth behavior revealing the direction of the target motion. The availability of this additional information is one of the main advantages of the laser self-mixing with respect to the classical interferometric techniques (e.g. Michelson or Mach-Zehnder interferometers).

In order to simultaneously measure target displacements with more than one degree of freedom (e.g. target displacements along the optical axis (longitudinal displacements), target displacements in the plane orthogonal to the optical axis (transverse plane), target rotations around the optical axis, etc..) one can either combine in suitable geometry two or more conventional diode lasers [3] or implement an array of mutually independent single transverse mode VCSEL [4–6]. In all these cases the sensing system is based on customized multi-sources assemblies.

A typical challenge to optical interferometry is the measurement of the purely transverse degrees of freedom of motion of the target, usually identified as straightness, flatness and roll. Several optical schemes have been proposed for measuring small roll rotations, possibly in combination with other degrees of freedom. They can be roughly divided into two categories, those relying on the polarization state of the laser radiation and those relying on tilting the wave vector with respect to the surface normal. Detection of roll angle by measurement of the phase shift between two orthogonal laser modes was demonstrated by Liu *et al.* [7] and the principle was further developed by Wu and Chuang [8]. However, additional phase sensitive optical elements must be inserted in the cavity and the heterodyne detection scheme requires two acousto-optic modulators for frequency shifting the laser mode. To the latter category belong all those detection schemes based on multiple laser sources aimed at pyramidal or prismatic reflective target [9–11]. These schemes also allow for multiple degrees of freedom measurements, however they suffer of limited resolution and/or limited angular range because of the geometrical boundaries.

Hence, the realization of a similar multi-tasking would be very interesting in terms of cost, compactness and riconfigurability, if attained with a single semiconductor laser emitting a more structured field, so that the multiplicity of measurements can be ascribed to the field/feedback

#156317 - $15.00 USD Received 11 Oct 2011; revised 9 Dec 2011; accepted 2 Jan 2012; published 5 Mar 2012

properties, rather than on the number of emitters. The simultaneous measurement of multiple target longitudinal displacements by self-mixing interferometry in a single laser diode has been recently reported by us [12]. However in [12] the laser was single mode (both longitudinal and transverse) and the target included independently moving parts.
Here, we introduce a model for laser whose emitted field is characterized by a number of transverse modes and we numerically investigate how the mode dynamics can respond in a viable fashion to the target feedback, so to allow for concurrent measurements of independent displacements.
More specifically, the idea is to link the spatial distribution of the transverse modes in the field profile of a mid-area semiconductor laser to the target degrees of freedom in such a way that the target motion would modify the spatial features of the feedback field distribution. The spectral properties of the transverse modes, in addition, cause a dynamical behavior that can in principle encode information on the target motion. In the applicative sections of this paper, we try to focus on the simplest regimes of a medium-aperture device where few families of transverse modes nonlinearly compete to rule the system dynamics. For such a scope, best candidates are the VCSEL with typical diameter of $10-20\mu m$. On the one side they benefit of low laser threshold, large-scale integrability, low cost and commercial proliferation. On the others side, their emission profile is known to be interpretable in terms of a few families of frequency degenerate transverse modes [13, 14]. Moreover, present techniques allow for a sophisticated engineering of their phase and/or intensity profiles by means of metal or dielectric grating, contact disc or ring, photonic crystal, etc... (see for example [15–17]). Although such structurations are not considered in this work, they can certainly represent a highly promising means to achieve an improved control of the device flexibility in acting as a sensor.

Whereas the complex transverse-mode behavior of VCSEL was mainly considered a drawback from the viewpoint of most applications oriented at optimizing the power emitted, the spectral stability or the operational bandwidth, they recently attracted a broad interest, especially since the control on VCSEL growth became accurate enough to put the modal structure under control (see for example [15–17])

On the one hand, there is a vast literature on the theoretical analysis of free running low- and mid- Fresnel number VCSEL dynamics in absence of external feedback (see for example [18, 19]). In all these cases the complex electric field profile is suitably described as the superposition of few linearly polarized Gauss-Laguerre or Bessel modes which may nonlinearly compete to give a regular spatio-temporal behavior (stationary patterns, mode-locking, self-pulsing, etc..). These phenomena of spatio-temporal self-organization can have in principle novel applications in the field of optical information processing. In fact, in the earliest stages of the field of "Transverse Nonlinear Optics" (see [20] and papers cited therein), a number of in-principle applications ranging from optical transistoring to associative memories were proposed, although in those days the technology was unripe for transfer to the VCSEL devices (see for example [21]). Other studies on transverse dynamics were proposed in the case of VCSEL modeling, including peculiarities such as field polarizations, residual anisotropies or spin flipping [22–24]. On the other hand, theoretical works based on the Lang-Kobayashi model [25] studied the semiconductor laser dynamics subjected to optical feedback in the plane wave approximation (i.e. assuming a transversely uniform field profile) in different feedback regimes. The effect of feedback on the laser characteristics depends on both the amount of the re-injected power and the round trip time of the field in the external cavity. The optical feedback may lead to stable single frequency emission or complex behaviors like chaotic intensity fluctuations or *Low Frequency Fluctuations* (see for example [1] and papers cited therein). The most interesting results for sensing applications have been obtained for weak or

#156317 - $15.00 USD Received 11 Oct 2011; revised 9 Dec 2011; accepted 2 Jan 2012; published 5 Mar 2012

moderate feedback regimes [1] where the laser emits on a single frequency at steady state. In this case, the interference fringes in the field intensity generated by the target motion along the optical axis are separated by $\lambda/2$.

There are relatively few works on the issue of optical feedback effects in a multi-transverse-mode VCSEL, as theoretically addressed for example in [26–28]. The authors consider an index guided device and expand the beam profile in the transverse plane in linearly polarized Bessel modes of the first and second kind in the core and the cladding respectively. In all these cases diffraction is neglected in the external cavity, and transverse mode degeneracy is either imposed or a frequency mode mismatch is introduced *ad hoc*. Moreover azimuthal modal dependence is often neglected to simplify the system dynamics and to relive the computations, thus reducing the problem to one transverse dimension. Where only few (two or three) rotationally symmetric modes are supposed to be excited, the modal competition is analyzed in detail and the works report the existence of single transverse mode operation, as well as mode-locking, like anti-phase or in phase dynamics of the modal intensities (see for example [27]). To the best of our knowledge, there have been no proposals for applicative schemes of such regimes.

In this paper, we cast a model suitable to provide a general description of the two dimensional spatio-temporal field dynamics in a transversally extended laser with moderate aperture with cylindrical symmetry, such as a graded index-guided VCSEL, subject to optical feedback. The cross size of the device is assumed to be such that the emission, at least not very far from threshold, can be described in terms of a few Gauss-Laguerre (GL) modes grouped in frequency degenerate families [18, 29]. The basic model is developed as to encompass multiple reflections from the external cavity and to account for laser-target settings exceeding a self-imaging configuration. We also allow for a spatially distributed feedback that can describe either a multi-sections external mirror or a mask in the external cavity. While the number of modes is in principle not limited by the approach, in the following analysis of the steady state regimes and laser dynamics, we prefer to restrict ourselves to a small number $(1-3)$ of linearly polarized modes, single reflection in the external cavity and self-imaging configurations, in order to maintain an intuitive picture of the modeling and identify new metrologically interesting properties of the reinjected device.

Focusing on the first frequency degenerate family of GL modes, we find parametric regimes where transverse mode-locking is found and we can in principle simultaneously and independently measure target longitudinal displacements and rotations in the transverse plane.

2. Model

The semiconductor laser dynamics, in presence of a spatially uniform feedback, has been widely described by the Lang-Kobayashi model, consisting of two coupled delayed rate equations for the amplitude of the electric field and the carriers density [25]. It holds in the single longitudinal mode and plane wave approximations and in the hypothesis of negligible multiple reflections in the external cavity between the laser exit facet and the target mirror. Its predictions for weak and moderate feedback are in very good agreement with a number of experimental evidences in the field of sensing and metrology [1].
Here we extend this model, to describe semiconductor laser multi-transverse-mode dynamics by making use of previously approaches developed in absence of optical feedback [18, 30–33], and to account for the presence of optical elements in the external cavity, as well as for multiple

#156317 - $15.00 USD Received 11 Oct 2011; revised 9 Dec 2011; accepted 2 Jan 2012; published 5 Mar 2012

reflections therein [26]. We also assume that the target mirror re-injecting to the laser may exhibit a deterministically designed spatial modulation of the reflectivity.

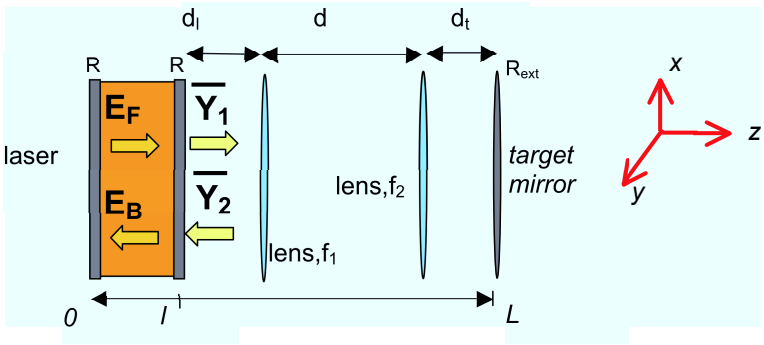

Fig. 1. Sketch of a semiconductor laser subject to optical feedback provided by an external target in a self-imaged configuration.

We consider a mid-area surface emitting semiconductor laser subjected to optical re-injection from an external reflecting target as sketched in Fig. 1. The resonator is supposed to exhibit cylindrical symmetry with respect to the propagation axis z with length l and radius r_c in the transverse (x,y) plane. The target mirror has complex reflectivity R_{ext} and is placed at a distance $L-l$ from the laser end facet whose mirror has in turn reflectivity R and transmissivity $T=1-R$. The two mirrors constitute a cavity, external with respect to the laser one, and we assume that two lenses in the external optical path make up a self-imaging configuration, so that diffraction in this path can be neglected. This requires of course a suitable choice of the lens focal lengths $f_{1,2}$, of their separation d and of the lens-laser d_d and lens-target d_t distances. A self-imaging configuration is realized for example when $f_1=f_2=f$, $d_l=d_t=f$, $d=2f$. E_F, E_B represent the forward and backward field envelopes respectively while $\bar{Y}_1$ and $\bar{Y}_2$ are the envelopes of the transmitted and injected fields that we suppose linearly polarized along a fixed direction in the transverse plane.
In presence of weakly index guiding in the transverse plane we assume a background refractive index that varies according to the law [18]:

$$n(r)=n(0)\sqrt{1-r^2/h^2}$$

where $n(0)=c\sqrt{\mu_0\varepsilon_0}$, $r=\sqrt{x^2+y^2}$ represents the radial coordinate and $h>>r_c$.

Expressed in terms of the forward and backward propagating fields introduced above, the field inside the laser cavity and the external cavity realized by the laser facet and the target mirror, are:

$$\begin{aligned} E(x,y,t) &= E_F(x,y,z,t)\exp(i(k_0z+\omega_0t))+E_B(x,y,z,t)\exp(i(-k_0z+\omega_0t))+c.c. \\ Y(x,yz,t) &= \bar{Y}_1(x,y,z,t)\exp(i(k_0'z+\omega_0t))+\bar{Y}_2(x,y,z,t)\exp(i(-k_0'z+\omega_0t))+c.c. \end{aligned}$$

where $\omega_0=-k_0'c=-k_0c/n(0)=-k_0\mathrm{v}$ is a reference frequency chosen arbitrarily, and v the light phase velocity in the medium.
In the slowly varying envelope approximations E_F and E_B satisfy the following paraxial Maxwell equations in the semiconductor medium [18]:

$$\frac{1}{2ik_0}\left(\nabla_\perp^2-\frac{k_0r^2}{h^2}\right)E_{F,B}\pm\frac{\partial E_{F,B}}{\partial z}+\frac{1}{\mathrm{v}}\frac{\partial E_{F,B}}{\partial t}=\frac{1}{2}g_n(1+i\alpha)(N-N_0)E_{F,B} \qquad (1)$$

#156317 - $15.00 USD Received 11 Oct 2011; revised 9 Dec 2011; accepted 2 Jan 2012; published 5 Mar 2012

The parameter g_n is the phenomenological gain coefficient, α is the Henry factor ($\simeq 1 \div 5$), $N(z,t)$ is the carrier density and N_0 its transparency value (typical value: $1.4 \times 10^{24} m^{-3}$).
We observe at this point that the "cold" eigenmodes of the empty laser cavity, which satisfy the equations obtained from Eq. (1) by setting equal to zero the coefficient g_n and the time derivatives, are given by [18]:

$$\mathscr{A}_{p,m}(\rho,\phi,z) = A_{p,m}(\rho,\phi)\exp(\mp i(2p+|m|+1)z/h)$$

where $\phi = tan^{-1}(y/x)$, $\rho = r/W_0 = r\sqrt{k_0}/\sqrt{2h}$ is a normalized radial coordinate and we introduced the Gauss-Laguerre modes of index $p = 0,1,2,3...,m = 0,\pm 1,\pm 2,\pm 3,..$:

$$A_{p,m}(\rho,\phi) = \sqrt{\frac{2}{\pi}}(2\rho^2)^{|m|/2}\left[\frac{p!}{(p+|m|)!}\right]^{1/2} L_p^{|m|}(2\rho^2)e^{-\rho^2}e^{im\phi} \tag{2}$$

In the previous expression $L_p^{|m|}$ are the generalized Laguerre polynomials (The functions $A_{p,m}$ are also the eigenmodes of a resonator with spherical mirrors in the limit $l << z_0$, where z_0 is the Rayleigh length [15, 30]).
The laser cavity eigenfrequencies are then:

$$\omega_{s,q} = \omega_s + \omega_q = \frac{\mathrm{v}}{l}s\pi + \frac{\mathrm{v}}{h}(2p+|m|+1) \tag{3}$$

where p and m are the transverse mode indices and $s = 0,1,2,...$ is the longitudinal mode index. It is important to observe that the frequency of the GL modes depends on the transverse index p and m only via the combination $q = 2p+|m|$, thus introducing degeneracy. The degenerate family of order q consists of $q+1$ modes. In the following the transverse modes of the cavity will be denoted by the couple of indices (p,m). In literature the mode $(0,0)$ is usually denoted as TEM_{00} while the modes $(0,\pm m)$ are indicated by TEM_{0m} and called doughnut modes because of their annular intensity distribution. From the limit $h >> l$, it directly follows that the frequency spacing between transverse modes $\Delta\omega_T = \mathrm{v}/h$ is much smaller than the longitudinal mode separation $\Delta\omega_L = \mathrm{v}\pi/l$. As it will be clear, this implies that even in the mean field limit that will be introduced soon, where a single longitudinal mode rules the system dynamics, several transverse modes can still compete to determine the dynamics of the transverse field profile.

Since the functions $A_{p,m}(\rho,\phi)$ form an orthonormal basis of the (ρ,ϕ) plane, the fields $E_{F,B}$ can be expanded as:

$$E_{F,B}(\rho,\phi,z,t) = \sum_{p,m}\varepsilon_{F,B;p,m}(z,t)\mathscr{A}_{p,m}(\rho,\phi,z), \quad \varepsilon_{F,B;p,m} \in \mathbb{C} \tag{4}$$

Inserting expressions (4) in Eqs. (1) and using the orthonormality of the Gauss-Laguerre functions we get:

$$\pm\frac{\partial\varepsilon_{F,B;p,m}}{\partial z} + \frac{1}{\mathrm{v}}\frac{\partial\varepsilon_{F,B;p,m}}{\partial t} = \frac{1}{2}g_n(1+i\alpha)\int_0^{2\pi}d\phi\int_0^{\infty}\rho d\rho\,\mathscr{A}^*{}_{p,m}(\pm z)(N-N_0)E_{F,B} \tag{5}$$

The boundary conditions at the two laser facets are:

$$\begin{aligned} E_F(x,y,z=0,t) &= \sqrt{R}E_B(x,y,z=0,t) \\ E_B(x,y,z=l,t) &= \sqrt{R}\exp(2ik_0l)E_F(x,y,z=l,t) + \sqrt{T}Y_2(x,y,z=l,t) \end{aligned}$$

we set $Y_2 = (\bar{Y}_2/\sqrt{n(0)})\exp(i(k_0-k_0')l)$. In terms of the modal amplitudes:

$$\begin{aligned} \varepsilon_{F;p,m}(0,t) &= \sqrt{R}\varepsilon_{B;p,m}(0,t) \\ \varepsilon_{B;p,m}(l,t) &= \sqrt{R}\exp(i\delta_0)\varepsilon_{F;p,m}(l,t) + \sqrt{T}Y_{2,p,m}(l,t) \end{aligned}$$

#156317 - $15.00 USD Received 11 Oct 2011; revised 9 Dec 2011; accepted 2 Jan 2012; published 5 Mar 2012

where we introduced the detuning $\delta_0 = \frac{2l}{\mathrm{v}}(\omega_q - \omega_0)$ and:

$$Y_2(\rho,\phi,z,t) = \sum_{p,m} Y_{2,p,m}(z,t)\mathscr{A}_{p,m}(\rho,\phi,-z), \quad Y_{2,p,m} \in \mathscr{C}$$

We now introduce the mean field limit as in [18] by assuming vanishing values for T, $g_n l$ and δ_0 and finite values for the ratios $\frac{g_n l}{\sqrt{T}}$ and $\theta = \frac{\delta_0}{\sqrt{T}}$.

In this approximation, which is very well verified in the case of VCSEL, the forward and backward field amplitudes are equal to their common average $E_{p,m}$ along z. We refer the reader to the Appendix for a complete treatment of the model in absence of limiting approximations; we report here the final integro-differential equations equation for the latter quantity:

$$\begin{aligned}\frac{dE_{p,m}}{dt} &= \left(iq\Delta\omega_T - \frac{1}{2\tau_p}(1+i\alpha)\right)E_{p,m} + \frac{1}{2}G_n(1+i\alpha)\int_0^{2\pi}d\phi\int_0^{\infty}\rho d\rho A^*_{p,m}(N-N_0)E \\ &+ \frac{1}{\tau_c}\int_0^{2\pi}d\phi\int_0^{\infty}\rho d\rho A^*_{p,m}k(\rho,\phi)E(\rho,\phi,t-\tau)\exp(-i\omega_0\tau) \qquad (6)\end{aligned}$$

where $\tau = 2L/c$ is the external cavity round trip and the feedback coefficient $k(\rho,\phi)$ is given by:

$$k(\rho,\phi) = \varepsilon\frac{(1-R)\sqrt{R_{ext}(\rho,\phi)}}{\sqrt{R}}$$

with the coefficient ε representing coupling losses per external cavity round trip or the effect of a neutral attenuator in the external cavity, as it is often the case in experiments. The dependence of the complex target reflectivity R_{ext} from the spatial variables will be particularly useful for modeling the experimental configurations exploiting spatially structured optical elements (e.g. spatial filters, phase masks, transversely modulated mirrors etc...). We have also introduced in Eq. (6) the cavity roundtrip time $\tau_c = \frac{2l}{v}$ (typical value: $8ps$), the photon life time $\tau_p = \frac{l}{\mathrm{v}T} + \alpha_m$ (typical value: $1.6ps$), $G_n = \frac{2g_n l}{\tau_c}$ (typical value: $8\times10^{13}m^3s^{-1}$). The coefficient α_m accounts for distributed linear losses in the laser cavity. The reference frequency is set as that of the free running, single longitudinal mode laser frequency ($\omega_0 = \omega_{\bar{s},0} + \alpha/2\tau_p$), where $\bar{s}$ identifies a particular longitudinal resonance. We observe that although our model is suitable to describe the most general case of multiple reflections as well as non self-imaging configuration, in writing Eq. (6) we restrict here to the simpler case of single external reflection and self-imaging configuration. While the second hypothesis allows us to neglect diffraction in the external cavity and corresponds to a specific choice of the optical system, the first one leads us to consider only weak or moderate feedback regimes, which are the most interesting for self-mixing interferometry.

The model is self-consistent when we add the rate equation for the carrier density:

$$\frac{dN(\rho,\phi,t)}{dt} = \frac{I}{eV} - \frac{N(\rho,\phi,t)}{\tau_e} - \frac{n(0)^2\varepsilon_0}{2\hbar\omega_0}G_n(N(\rho,\phi,t)-N_0)|E(\rho,\phi,t)|^2 \qquad (7)$$

with I = pump current, e = electron charge and V = volume of the active region. τ_e is the carrier decay time (typical value: $\sim 1ns$). Note that Eqs. (6)-(7) reduce to the well known Lang-Kobayashi model [25] in the plane wave approximation and spatially uniform feedback.

To obtain adimensional relations we adopt the following scaling:

$$\sqrt{\frac{G_n\tau_e n(0)^2\varepsilon_0}{2\hbar\omega_0}}E \to E, \quad (N-N_0)G_n\tau_p \to N, \quad t/\tau_p \to t$$

$$\chi(\rho) = I_p e^{-2\rho^2/\Psi^2}, \quad \Psi \in \mathscr{R} \quad \text{with} \quad I_p = G_n\tau_p N_0\left(\frac{I\tau_e}{eVN_0} - 1\right), \quad \gamma = \frac{\tau_p}{\tau_e}$$

#156317 - $15.00 USD Received 11 Oct 2011; revised 9 Dec 2011; accepted 2 Jan 2012; published 5 Mar 2012

where we assume that the spatial dependent pump $\chi(\rho)$ has a gaussian shape. The modal amplitude rate equations now read:

$$\frac{dE_{p,m}(t)}{dt} = \left(iq\Delta\omega_T\tau_p - \frac{1}{2}(1+i\alpha)\right)E_{p,m}(t) + \frac{1}{2}(1+i\alpha)\int_0^{2\pi}d\phi\int_0^{\infty}\rho d\rho A^*_{p,m}N(\rho\phi,t)E(\rho\phi,t)$$
$$+ \frac{\tau_p}{\tau_c}\int_0^{2\pi}d\phi\int_0^{\infty}\rho d\rho A^*_{p,m}k(\rho,\phi)E(\rho,\phi,t-\tau)\exp(-i\omega_0\tau) \quad (8)$$

$$\frac{dN(\rho\phi,t)}{dt} = \gamma\left(\chi(\rho) - N(\rho\phi,t)(1+|E(\rho\phi,t)|^2)\right) \quad (9)$$

The general form of the pump is suitable to describe both optically and electrically pumped VCSEL, inasmuch in [34] the authors showed that current crowding has little effect on the pattern structures as long as the cylindrical symmetry is preserved.
It is computationally preferable to work with sets of real equations, so that we introduce the linear combination of Gaussian-Laguerre functions (Eq. (2)) defined as:

$$B_{p,m,0}(\rho,\phi) = A_{p,0}(\rho,\phi)$$
$$B_{p,m,1}(\rho,\phi) = \frac{1}{\sqrt{2}}\left[A_{p,m}(\rho,\phi) + A_{p,-m}(\rho,\phi)\right]$$
$$B_{p,m,2}(\rho,\phi) = \frac{1}{\sqrt{2}i}\left[A_{p,m}(\rho,\phi) - A_{p,-m}(\rho,\phi)\right]$$

Accordingly the angular index m takes only non-negative values. Obviously the eigenfrequencies are still given by Eq. (3) and the frequency degeneracy of each q family is still $q+1$. Since $B_{p,m,o}$ are real functions, this substitution allows for a straightforward separation of equations (8)-(9) in real and imaginary parts. Furthermore in terms of the new basis:

$$E(\rho,\phi,t) = \sum_{p,m,o} g_{p,m,o}(t)B_{p,m,o}(\rho,\phi), \quad g_{p,m,o} \in \mathscr{C}$$

The intensity distribution of the $B_{p,m,o}$ modes is reported for example in Fig. 3 of [33]. In order to simplify the notation we replaced in the following the modal indices $\{p,m,o\}$ with the single progressive index i.

3. Numerical simulations

In this section we report the results of extended numerical simulations of the field dynamics. As it can be easily understood, the competition among several frequency spaced mode families (each one beating in frequency) coupled to the spatial hole burning due to the (x,y) field profiles, often leads to chaotic dynamics. Here we start by showing that there exist domains of transverse mode-locking, leading to a periodic regime, one above the free running laser (FRL) threshold in the case of *weak* feedback and the other below the FRL threshold for *strong* feedback. In the next section we will show how in these cases the information encoded in the field profile can be exploited to simultaneously and independently measure target displacements with more than one degree of freedom.
We preliminary performed a wealth of checkpoints on the laser without feedback, in order to reproduce results obtained in literature for GL-multimode lasers [33].
We numerically integrated the modal amplitudes equations derived in the previous section Eqs. (8)-(9) by implementing an accurate and efficient numerical algorithm based on $6th$ order Adams-Bashforth-Moulton predictor-corrector method. The integrals were computed by the Gaussian quadrature method.

#156317 - $15.00 USD Received 11 Oct 2011; revised 9 Dec 2011; accepted 2 Jan 2012; published 5 Mar 2012

3.1. *Laser transverse dynamics in presence of uniform external feedback*

In the case of interest we mainly investigated the dynamics of the two $(q=1)$ frequency degenerate modes for different values of the feedback strength k and the pump I_p at a fixed feedback delay time τ given by the external cavity length L ($\tau = 2L/c$).
In Fig.2(a) we summarize our most significant results for $\tau = 0.16ns$ which corresponds to an external cavity of $L = 2.4cm$. In this figure, as in the following ones, we adopt the physical units for the time t and longitudinal coordinate z. The red crosses represent the values of k and I_p considered in the simulations. We were able to distinguish five different dynamical domains denoted by the letters A, B, C, D, E and depicted in Fig.2(a).
As described in the following, we observed a regular system dynamics only in region A and D. The former corresponds to weak or very weak feedback ($k < 0.01$) and pump I_p above the FRL threshold ($I_p > 1$), the latter corresponds to strong feedback ($k > 0.1$) and I_p slightly below (less than $\simeq 15\%$) the FRL threshold. In the regions B and C the mode competition always leads to an irregular dynamics. In the region E the feedback is insufficient to trigger lasing emission.Although we did not perform a systematic study, we noted that the extension of the different dynamical domains in the (k, I_p) plane varies with τ but maintains the same qualitative appearance.

3.1.1. Dynamics of the $(q=1)$ frequency degenerate family. Above the FRL threshold.

For $k = 0$ (no feedback) the two modes oscillate regularly in anti-phase with average value, amplitude and Fourier spectrum which depend on I_p.We interpret this in terms of spatial hole burning, causing the carrier density and the gain to increase where the field intensity is smaller so that the system tries to change the lasing regions as proposed in [31, 35]. It follows that the

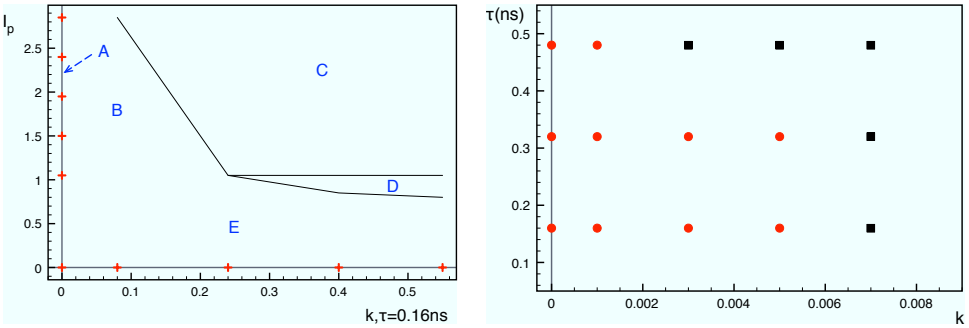

(a) (b)

Fig. 2. Parametric regime: $\alpha = 5$, $\alpha_0 = 3.0$, $\Psi = 50.0$, $\gamma = 0.001$. (a) $\tau = 0.16ns$. Summary of the numerical results in the (k, I_p) plane for the family $(q=1)$. The red crosses represent the values of k and I_p considered in the simulations. The vertical and horizontal gray lines denote the $k = 0$ and $I_p = 0$ axis. The different dynamical domains A, B, C, D and E separated by the black continuous lines are described in the text. The red crosses corresponding to region A are not shown in the picture for sake of clarity. (b) $I_p = 1.05$. Each symbol represents a numerical simulation. The red circles correspond to regular oscillations of the field intensity while the black squares are associated to an irregular dynamical behavior.

frequency of this periodic dynamics must be close to the relaxation oscillation frequency which is $\omega_r = \sqrt{\gamma(I_p - 1)}$ at the lowest oder in γ. The fact that the anti-phase dynamics has been also reported in different models like those in [26, 27] indicates that this is a robust dynamical

#156317 - $15.00 USD Received 11 Oct 2011; revised 9 Dec 2011; accepted 2 Jan 2012; published 5 Mar 2012

feature of the system.
In region B a continuum of new frequencies is present in the power spectrum. For increasing values of I_p the width and height of the Fourier spectrum maximum increases and blue-shifts towards the closest external cavity resonance $\omega_1 = 2\pi/\tau$.
In region C we observe that the number of peaks in the FFT increases by increasing k showing again an irregular system dynamics (see for example Fig.3(a)). The central frequencies of their envelopes gradually shift towards the closest external cavity resonances while their linewidths decrease accordingly.

Above the FRL threshold we observed a phase-locking dynamics only in region A, i.e. when the feedback strength k is smaller than a critical value. This is confirmed by the results in Fig.2(b) which also show that the critical k depends on τ.
We plot in the left panel of Fig.3(b) the modal intensity evolution of the two $(q = 1)$ modes, TEM_{10} (B_2) and TEM_{01} (B_3), at steady state. In the inset we can see the averaged $(50ns)$ intensity profile of each mode and of the total intensity (sum of the modal intensities). The two modes evolve with a frequency close to the relaxation oscillation frequency (see right panel of Fig.3(b)). Note that they are not exactly in anti-phase since the total intensity, is not constant in time. As expected the departure from the perfect anti-phase dynamics reduces by increasing the photon-to-carrier lifetime ratio γ, i.e. by reducing the spatial hole burning characteristic time scale. Moreover, as it happens in absence of feedback $(k = 0)$, the average value and the amplitude of these periodic oscillations increase with the pump I_p.

3.1.2. Dynamics of the $(q = 1)$ frequency degenerate family. Below the FRL threshold.

Below the FRL threshold and for sufficiently high feedback strength we found region D where the system exhibits again regular anti-phase oscillations with a frequency that approaches the cavity resonance $2\pi/\tau = 39.27GHz$ (see Fig.3(c)). This evidence might be explained if we consider an effective photon-to-carrier lifetime ratio, and consequently an effective relaxation oscillation frequency, calculated assuming the cavity length equal to the external cavity's. Being the new relaxation frequency much larger, we can thus expect the mode competition to be ruled by the new, slower time scale that becomes the effective cavity round trip time τ. Moreover we note that the amplitude and average value of the periodic oscillations increase with the pump I_p and at regime the mode with higher intensity is determined by the initial noise distribution. We plan to further investigate the process of generation of a periodic modal intensity oscillation at a frequency much higher than the typical semiconductor laser relaxation's (few GHz) because of its potential applications into the field of optical communication (see for example [36]).

3.1.3. Dynamics of $q = 2$ frequency degenerate family.

As already stated in Sections 1 and 2, our model is suitable to describe the competition among an arbitrary number of transverse modes, thus we devoted a limited number of simulations looking for mode-locking phenomena when the 3 frequency degenerate modes of the $q = 2$ family are active. In general, here the dynamics is irregular but we were able to identify special conditions where a transverse mode-locking can be found provided that the mode with central maximum (B_4 mode) is suppressed. In this case the remaining B_5 and B_6 modes, which breaks the azimutal symmetry, evolve in anti-phase and we may in principle extend to this case all the results reported in the next section about simultaneous measurements of target displacements valid for the TEM_{10} (B_2) and TEM_{01} (B_3) in the phase-locking regime.

#156317 - $15.00 USD Received 11 Oct 2011; revised 9 Dec 2011; accepted 2 Jan 2012; published 5 Mar 2012

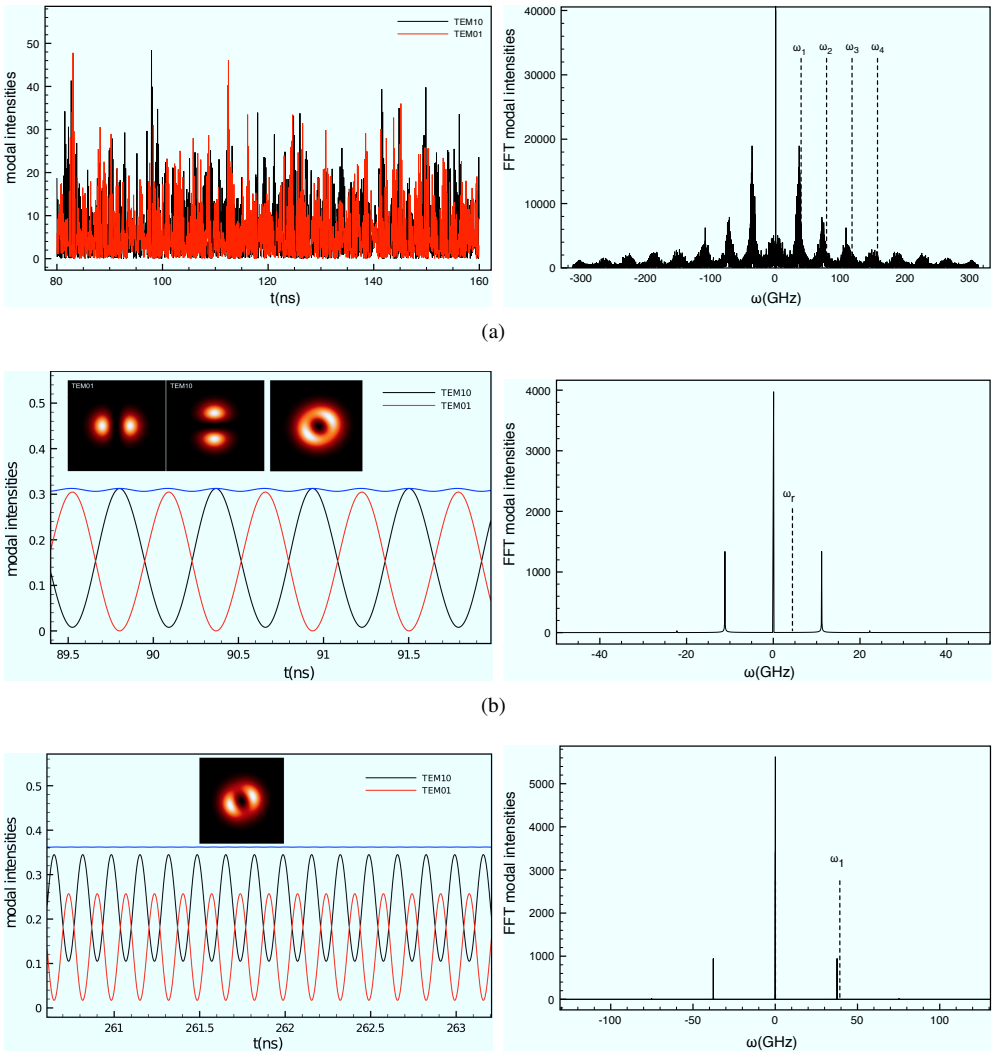

Fig. 3. Parametric regime: $\alpha = 5$, $\alpha_0 = 3.0$, $\Psi = 50.0$, $\gamma = 0.001$, $\tau = 0.16ns$. (a) Region C ($I_p = 2.4$, $k = 0.4$). Left: Temporal evolution of the modal intensities of the TEM_{10} (B_2) and TEM_{01} (B_3) modes. Right: Fast Fourier trasform (FFT) of the TEM_{10} modal intensity. We plot the FFT of a single transverse mode, the FFT of the other mode is analogous. The dashed lines denote the external cavities resonances ω_i. (b) Region A ($I_p = 1.05$, $k = 0.0008$) and (c) Region D ($I_p = 0.9$, $k = 0.4$). Left: Temporal evolution of the modal intensities of the TEM_{10} and TEM_{01} modes. The blue trace represents the sum of the modal intensities. The intensity profile of the two modes is reported in the inset together with the total intensity distribution averaged over $\sim 50ns$. The dimension of the transverse plane is $5W_0 \times 5W_0$ in the simulation. Right: FFT of the TEM_{10} modal intensity. The dashed line in part (b) denotes the relaxation oscillation frequency ω_r while in part (c) it denotes the first external cavity resonance.

#156317 - $15.00 USD Received 11 Oct 2011; revised 9 Dec 2011; accepted 2 Jan 2012; published 5 Mar 2012

We finally observe that when the six transverse modes of the $(q = 0)$, $(q = 1)$ and $(q = 2)$ families compete to rule the system dynamics we may get a phase-locking regime provided large losses are added to the modes that gain in the central region (B_4 and B_0 modes). This suggests that for a VCSEL emitting several mode families (as it is often the case with off-the-shelf commercial multimode VCSELs), a locking regime might be found among modes with $m \neq 0$, if one can suppress the modes with axial maxima.

4. Applications to displacements measurements

In this section, we exploit the complex features of the field emitted by a multimode mid-area VCSEL, as considered above, for the simultaneous measure of target longitudinal displacements and target rotations around the optical axis. To reach this goal we use the dynamical properties and the spatial distribution of the TEM_{01} and TEM_{10} modes in the regimes discussed in the previous section.

4.1. Simultaneous measure of target rotations in the transverse plane and target longitudinal displacements using spatially modulated feedback

The need to relay on regular mode dynamics, limits us to the two regions *A* and *D* in Fig. 2(a). We note that physically the latter regime requires a high k and this implies a laser with a low internal mirror reflectivity ($R < 0.5$) as can be achieved in optically pumped devices [37] or in VCSEL with anti an reflection coating (e.g. those found in VECSEL devices) [38]. We chose to investigate this regime first and more in depth since the modal behavior under feedback is simpler and the measurements are cleaner and better understood. Nevertheless, for commercial VCSEL with electrical pumping (we recall that the role and shape of the pump in our model (section 2) is quite general) the high reflectivity ($R > 0.95$) leads to much lower values of k. In this case the available operational regime is that corresponding to region *A*. At the end of this section we show that the same measurement technique remains unchanged and can be performed in a similar way with analogous results, although a reduced sensitivity is predicted.

4.2. Measure of target rotations in the transverse plane

In order to make our device sensitive to target rotations in the transverse plane, we now assume that the target mirror is not uniform but has a spatial modulation of its reflectivity such as that sketched in Fig.4(a). The two white quarters of the circle correspond to $k = 0$ (i.e. there is no reflection), while in the gray parts $k = 0.4$. The mirror is then rotated by steps of $\Theta = 0.17 rad$ each $32 ns$ around the optical axis. As Fig.4(a) shows, for each target rotation step we observe a clear jump in the intensities of the TEM_{10} and the TEM_{01} modes that corresponds to the rotation of the field profile shown in the bottom panel of Fig.4(a). The steep slopes following each rotation define the fastest response time of the system in the *ns* range ($\sim \tau_e$), corresponding to a maximum detectable rotation frequency of about 50 MHz (see Fig 4b). Although such upper limit is not achievable in a mechanical rotator, we note that the steady state reached afterwards by the system (after some ringing) ensures that much slower rotation frequencies will be equally detected.

We observe at this point that the proposed system is not able to detect the direction of the target rotation. Of course one could think to realize more complex spatial profiles for the feedback masks, e.g. by breaking the clockwise-anticlockwise symmetry, which would change the spatial hole burning process for either TEM01 and TEM10 mode in a different way for clockwise and anticlockwise target rotations, thus allowing to discriminate between the two.

#156317 - $15.00 USD Received 11 Oct 2011; revised 9 Dec 2011; accepted 2 Jan 2012; published 5 Mar 2012

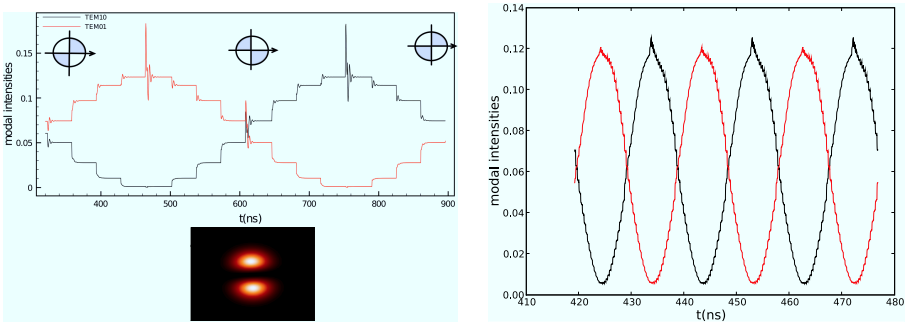

(a) (b)

Fig. 4. Parametric regime as in Fig.3(c). (a) Top: Time plot of the modal intensities during a feedback mask rotation from $\Theta = 0$ (left inset mask) to $\Theta = \pi$ (right inset mask) (rotation steps of $\Theta = 0.17rad$ each $32ns$). Bottom: Single frame extracted from the numerical simulation of the field intensity variation (Media 1. (b) Time plot of the modal intensities during a feedback mask rotation from $\Theta = 0$ to $\Theta = 3\pi$ (rotation steps of $\Theta = 0.05rad$ each $0.32ns$).

4.3. Measure of target displacement in the longitudinal direction

In the same parametric regime, in presence of spatially uniform feedback, we proved the device sensitivity to longitudinal displacements of the target. Our results are reported in Fig.5(a) and Fig.5(b). In Fig.5(a) we plot the variation of the highest peak frequency in the FFT of the modal intensities versus the target longitudinal displacement dL. We start with an external cavity length $L = 2.4cm$, which corresponds to $dL = 0$, where the modal intensities oscillate at a frequency close to the first cavity resonance of $\sim 39GHz$. By gradually increasing dL we observe at $dL \sim \frac{\lambda}{4}$ a sudden change in the FFT peak position which becomes $\sim 3GHz$. This change is periodic with the target shift and allows to measure translations with the same $\frac{\lambda}{2}$ accuracy as the standard self-mixing methods; the frequency shift, though, does not allow to discriminate between the directions of the translation. We attempt as an explanation for this frequency discontinuity, observing that the frequency discontinuity we observe that when the length L of the external cavity is different from an odd integer multiple of $\simeq \lambda/4$ the presence of the dominant frequency peak at around the inverse of the first cavity resonance might be justified as in paragraph 3.1.2: the system is assimilated to a laser with effective cavity equal to the external one. On the contrary, when L is an odd integer multiple of $\simeq \lambda/4$ the interference is almost destructive and we may expect that the oscillations of the modal intensities to drop towards the relaxation oscillation frequency, thus showing a dominant low frequency peak.

In Fig.5(b) we plot the average total intensity versus target longitudinal displacement dL. It is easy to identify the $\lambda/2$ periodicity typical of feedback interferometry when measuring displacements. As in standard self-mixing (single transverse mode lasers) the intensity shift allows to discriminate between the directions of the translation.

The previous results show that, contrary to what happens in the case of a conventional laser diode emitting a single transverse mode, at least two different *quantifiers* can be potentially associated with a measure of the target longitudinal displacements with a submicrometric resolution: the average total intensity (as in the single mode laser diode) and the frequency of the modal intensity oscillations.

#156317 - $15.00 USD Received 11 Oct 2011; revised 9 Dec 2011; accepted 2 Jan 2012; published 5 Mar 2012

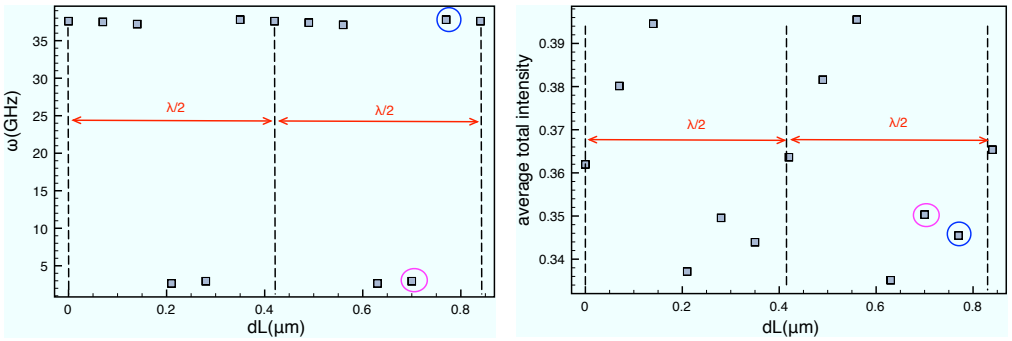

(a) (b)

Fig. 5. Parametric regime: $\alpha = 5$, $\alpha_0 = 3.0$, $\Psi = 50.0$, $\gamma = 0.001$, $I_p = 0.9$, $k = 0.4$. (a) Primary (low frequency) peak variation in the FFT of the TEM_{10} modal intensity (that of TEM_{01} mode is very similar) with the displacement dL. (b) Variation of the average total intensity with the displacement dL. The circles highlight the frequency discontinuity and the corresponding values of the average total intensity.

4.4. Concurrent measurements of multiple target displacements: target rotations in the transverse plane and target longitudinal displacements

The multiple informations encoded in the multimode field profile reported in the previous paragraphs seem to indicate the possibility to simultaneously measure different target displacements, i.e. target displacements with more than one degree of freedom.
To prove this we considered again a structured target mirror like that sketched in Fig.4(a) and plot in Fig.6 the sum of the modal intensities, $I_{sum}=|g_1|^2+|g_2|^2$, and the normalized difference, $I_{diff}=(|g_1|^2-|g_2|^2)/I_{sum}$, during a target rotation of $\pi/2$ in the transverse plane for a fixed external cavity length (Fig.6(a)) and a target longitudinal displacement of $1\mu m$ for a fixed angular position of the mask (Fig.6(b)). We see that I_{sum} is not affected by the rotation, while I_{diff} allows to measure the rotation steps, while on the contrary, during the translation I_{sum} quantifies the motion while the I_{diff} remains unaffected. This clearly shows that the two quantities represent a couple of suitable quantifiers of multiple target displacements.

As anticipated in the beginning of this section we get similar results also above the FRL threshold where transverse mode-locking occurs. The results are reported in Fig.7.
An inspection of Fig.7(a) and Fig.7(b) shows that the quantity I_{diff} oscillates at a frequency close to the relaxation oscillation frequency, contrary to what happens below the FRL threshold (see Fig.6). Nonetheless, by low-pass filtering the I_{diff} temporal trace, as shown in Fig.7(c), we still get a proper measure of the rotational steps of the target. From an experimental point of view this corresponds to use a "slow" detector to measure I_{diff}. Moreover, as observed below the FRL threshold, the quantity I_{sum} remains unchanged by the rotation.
Slightly different is the situation regarding the measurement of target translation (see Fig.7(d)). The half wavelength periodicity in the I_{sum} signal is still evident, but the contrast is reduced by roughly a factor 2. The quantity I_{diff} is not constant, but exhibits a slight modulation ($< 1.5\%$) which is anyway much smaller than the mean value jumps due to rotation. Thus, such a side effect cannot shade out the independence of the two quantifiers with respect to the two target motions.

#156317 - $15.00 USD Received 11 Oct 2011; revised 9 Dec 2011; accepted 2 Jan 2012; published 5 Mar 2012

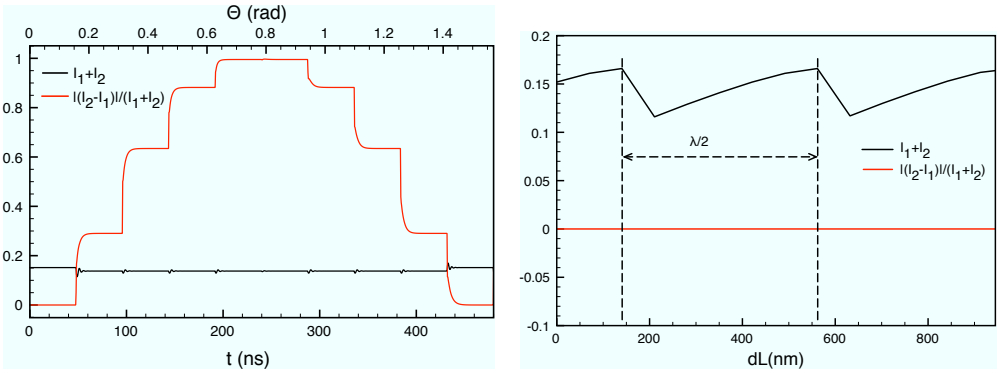

(a) (b)

Fig. 6. Parametric regime: $\alpha = 5$, $\gamma = 0.001$, $I_p = 0.9$, $k = 0.4$. Modal intensities sum (I_{sum}) and normalized difference (I_{diff}) during: (a) a target rotation of $\pi/2$ in the transverse plane for a fixed external cavity length $L = 2.4cm$ (We rotate the feedback mask of $\Theta = 0.17rad$ each $48ns$); (b) a target longitudinal displacement of $1\mu m$ ($dL = 0$ corresponds to $L = 2.4cm$, $\lambda = 830nm$) for a fixed angle $\Theta = 0rad$.

A comment is in order to address the actual experimental realization and benefit of the proposed scheme.

First of all, the requirement of a cooperative target, like a structured mirror, is necessary to avoid speckle interference, but will restrict the range of possible applications. Speckles arising from using a diffusive target would most probably disrupt the mode dynamics especially in the case of frequency degenerate modes. Although most laser self-mixing applications operate with diffusive surfaces, a number of relevant applications have been demonstrated for mirror like target (see for example [3, 39–41]).

As far as the laser source is concerned, small-size VCSEL with few GL modes competing just above threshold are readily commercially available. However, the residual birefringence of the device structure usually breaks the intrinsic cylindrical symmetry of the system in such a way that the GL modes belonging to the same family are no longer frequency degenerate and have orthogonal polarizations. Nevertheless there are critical points in the injection current/temperature parameter space (the polarization switching points) where $TEM01$ and $TEM10$ modes are simultaneously lasing with the same average power (see for example [24]). Their different polarization would thus make experimentally easier the independent measurement of their individual power required to calculate the sum and difference I_{sum} and I_{diff}. The response time of the system averaged over $1\mu s$ would allow rotation speed measurement up about $10^5 rpm$ by counting the oscillation frequency of any of the two modes (as in Fig. 4(b)). At the same time, any possible longitudinal displacement of the target could be detected with sub-wavelength resolution by measuring the total power modulation (as in Fig. 6(b) and Fig. 7(d)). High precision drilling and milling applications could possibly benefit from resorting to a single device to control both rotation speed and penetration depth. Second, while the conventional self-mixing system, based on a laser diode or on a single longitudinal mode VCSEL, only requires the reading of the internal photodiode current, or even just terminal voltage variation, the proposed scheme, based on a multimode VCSEL, introduces a mechanical complication given by the presence of a polarizing beam-splitter and two external detectors. However, such a technical drawback is rewarded by having simultaneous access to two different degrees-of-freedom of motion with a single device, the revolution speed being also entirely in the transverse

#156317 - $15.00 USD Received 11 Oct 2011; revised 9 Dec 2011; accepted 2 Jan 2012; published 5 Mar 2012

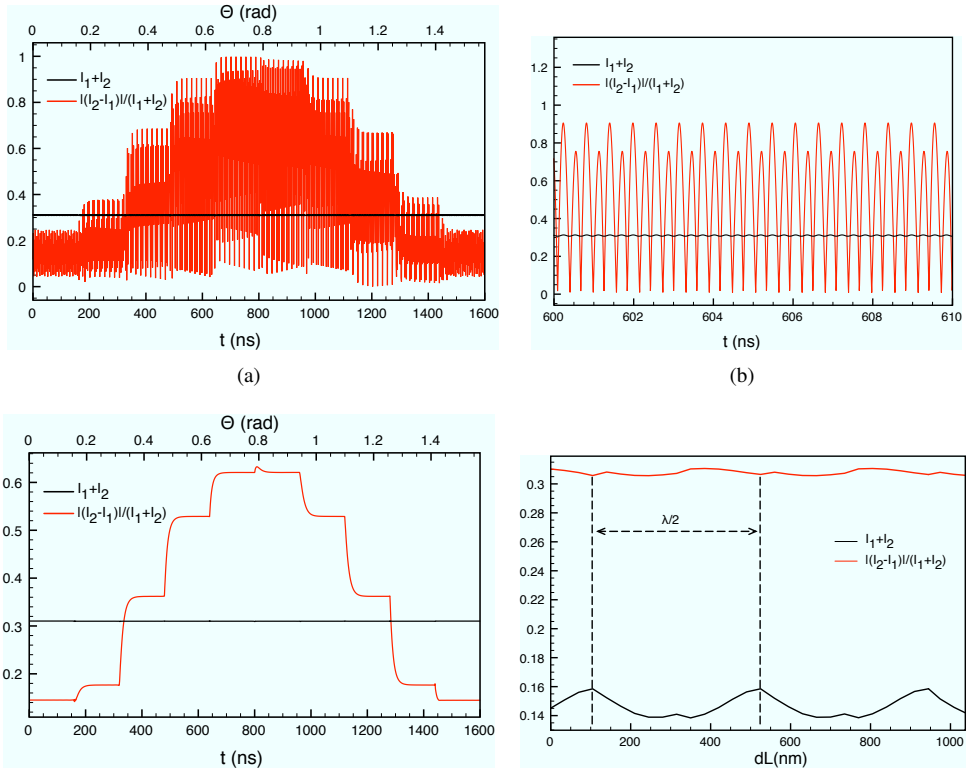

Fig. 7. Parametric regime: $\alpha = 5$, $\gamma = 0.001$, $I_p = 1.05$, $k = 0.002$. Plot of I_{sum} and I_{diff} during: (a) a target rotation of $\pi/2$ in the transverse plane for a fixed external cavity length $L = 2.4cm$ (We rotate the feedback mask of $\Theta = 0.17rad$ each $160ns$); (d) a target longitudinal displacement of $1\mu m$ ($dL = 0$ corresponds to $L = 2.4cm$, $\lambda = 830nm$) for a fixed angle $\Theta = \pi/4$. In part (a) for sake of clarity not all the data points in the I_{diff} trace are plotted. The plot in part (b) represents a zoom of the traces in part (a). Figure 7(c) has been obtained by low-pass filtering the oscillations shown in part (a) with a cut-off at $1MHz$, corresponding to a detector integration time of about $1\mu s$.

#156317 - $15.00 USD Received 11 Oct 2011; revised 9 Dec 2011; accepted 2 Jan 2012; published 5 Mar 2012

plane, a plane typically unaccessible by interferometric measurements.
Finally, since spatially filtered optical feedback is already a widely used technique to stabilize the mode emission in multimode VCSELs [17] as well as in broad-area diode lasers [42], we believe that the proposed detection method could be experimentally implemented using commercial devices, attaining mode control as well as two degrees of freedom measurement capability at the same time.

5. Conclusions

In conclusion we developed a general model to describe the effect of spatially structured feedback on mid-area semiconductor laser which quite generally describes the dynamics of an arbitrary number of transverse and longitudinal modes. For simplicity and in order to demonstrate applicative potentials of such systems, we reported results in the case of single reflection, self-imaging external cavity, mean field approximation (single longitudinal mode) and we limit the number of transverse modes to two (first family of frequency degenerate modes). Our simulations reveal the existence of dynamical regimes of transverse mode-locking where informations on target longitudinal displacements and target rotations in the transverse plane are easily and independently encoded in the phase and/or amplitude field profile by introducing a spatially structured feedback mirror. This indication is thus very promising for applications in metrology since would allow to conceive a single-emitter device to simultaneous measure target motion with different degrees of freedom.

Appendix

In this Appendix we report the detailed derivation of the equation (6) that describes the dynamics of a mid-area semiconductor laser, e.g. a VCSEL, subjected to optical feedback in the mean field limit.
Introduced the auxiliary field amplitudes:

$$\begin{aligned}\varepsilon'_{F;p,m} &= \exp(i\delta_0+\ln(\sqrt{R})(z-l)/l)\varepsilon_{F;p,m}+\frac{z}{l}\frac{\sqrt{T}}{\sqrt{R}}Y_{2,p,m}\\ \varepsilon'_{B;p,m} &= \exp(-\ln(\sqrt{R})z/l)\varepsilon_{B;p,m}\end{aligned}$$

which obey the periodic boundary conditions:

$$\varepsilon'_{F;p,m}(0,t) = \varepsilon'_{B;p,m}(0,t) \quad (10)$$

$$\varepsilon'_{F;p,m}(l,t) = \varepsilon'_{B;p,m}(l,t) \quad (11)$$

#156317 - $15.00 USD Received 11 Oct 2011; revised 9 Dec 2011; accepted 2 Jan 2012; published 5 Mar 2012

we can recast Eqs. (5) as:

$$\frac{\partial \varepsilon'_{F;p,m}}{\partial z}+\frac{1}{\mathrm{v}}\frac{\partial \varepsilon'_{F;p,m}}{\partial t}-\frac{z}{l}\frac{\sqrt{T}}{\sqrt{R}}\frac{\partial Y_{2,p,m}}{\partial z}-\frac{z}{vl}\frac{\sqrt{T}}{\sqrt{R}}\frac{\partial Y_{2,p,m}}{\partial t}=\frac{\sqrt{T}}{l}\Big(\left(\varepsilon'_{F;p,m}-\frac{z}{l}\frac{\sqrt{T}}{\sqrt{R}}Y_{2,p,m}\right)\left(\frac{i\delta_0}{\sqrt{T}}+\frac{\ln(\sqrt{R})}{\sqrt{T}}\right)$$
$$+\Big(\frac{l}{2\sqrt{T}}g_n(1+i\alpha)\sum_{p',m'}\left(\varepsilon'_{F;p',m'}-\frac{z}{l}\frac{\sqrt{T}}{\sqrt{R}}Y_{2,p',m'}\right)\exp\left(\frac{-2i(q'-q)z}{h}\right)$$
$$\int_0^{2\pi}d\phi\int_0^{\infty}\rho d\rho\mathscr{A}^*{}_{p,m}(z)\mathscr{A}_{p',m'}(z)(N-N_0)\Big)+\frac{Y_{2,p,m}}{\sqrt{R}}\Big) \tag{12}$$

$$-\frac{\partial \varepsilon'_{B;p,m}}{\partial z}+\frac{1}{\mathrm{v}}\frac{\partial \varepsilon'_{B;p,m}}{\partial t}=\frac{\sqrt{T}}{l}\Big(\varepsilon'_{B;p,m}\frac{\ln(\sqrt{R})}{\sqrt{T}}$$
$$+\left(\frac{l}{2\sqrt{T}}g_n(1+i\alpha)\sum_{p',m'}\varepsilon'_{B;p',m'}\int_0^{2\pi}d\phi\int_0^{\infty}\rho d\rho\mathscr{A}^*{}_{p,m}(-z)\mathscr{A}_{p',m'}(-z)(N-N_0)\right)\Big) \tag{13}$$

We chose as reference frequency that of the fundamental Gaussian mode of given longitudinal index $\bar{s}$ ($\omega_0=\omega_{\bar{s},0}$) and we additionally suppose valid the mean field limit, i.e. small laser facets transmission, small gain per cavity round trip and small cavity detuning. Under this approximation by summing up side by side Eqs. (12)-(13), taking the average along z and using the boundary conditions (10)-(11):

$$\frac{dE_{p,m}}{dt}=\frac{\mathrm{v}\sqrt{T}}{2l}\left(E_{p,m}\left(i\theta-\sqrt{T}\right)+\frac{l}{\sqrt{T}}g_n(1+i\alpha)\int_0^{2\pi}d\phi\int_0^{\infty}\rho d\rho A^*_{p,m}(N-N_0)\bar{E}+\frac{Y_{2,p,m}}{\sqrt{R}}\right)$$

where we supposed that $E_{p,m}=\frac{1}{l}\int_0^l\varepsilon'_{F;p,m}dz\simeq\frac{1}{l}\int_0^l\varepsilon'_{B;p,m}dz$, that the carrier density N is almost constant along z and we set $\bar{E}(\rho,\phi)=\sum_{p,m}E_{p,m}A_{p,m}(\rho,\phi)$. These latter two hypothesis are very well verified in a semiconductor laser cavity with a longitudinal dimension of few microns like a VCSEL.
After renaming E the field $\bar{E}$ we finally get the following system of coupled, nonlinear, integro-differential equations for the field modal amplitudes:

$$\frac{dE_{p,m}}{dt}=\left(iq\Delta\omega_T-\frac{1}{2\tau_p}(1+i\alpha)\right)E_{p,m}+\frac{1}{2}G_n(1+i\alpha)\int_0^{2\pi}d\phi\int_0^{\infty}\rho d\rho A^*_{p,m}(N-N_0)E+\frac{\sqrt{T}}{\sqrt{R}\tau_c}Y_{2,p,m} \tag{14}$$

where we reset the reference frequency as the free running, single longitudinal mode laser frequency ($\omega_0=\omega_{\bar{s},0}+\alpha/2\tau_p$) and we exploit the relation $\omega_{\bar{s},q}-\omega_{\bar{s},0}-\alpha/2\tau_p\simeq\omega_{\bar{s},q}-\omega_{\bar{s},0}=q\Delta\omega_T$.
In order to account for multiple reflections in the external cavity one may write:

$$\begin{aligned}Y_2(l,t) &= \frac{\exp(i(k_0-k'_0)l)}{\sqrt{n(0)}}\bar{Y}_2(l+L,t-\tau/2)\exp(-2ik'_0L)\\ &= \sqrt{R_{ext}}\sqrt{1-R}\exp(2ik_0l)\exp(-i\omega_0\tau)E_F(l,t-\tau)-\sqrt{R_{ext}}\sqrt{R}\exp(-i\omega_0\tau)Y_2(l,t-\tau)\end{aligned}$$

According to the mean field limit we can set:

$$Y_2(l,t)=\varepsilon\sqrt{R_{ext}}\sqrt{1-R}\exp(-i\omega_0\tau)E(t-\tau)-\varepsilon\sqrt{R_{ext}}\sqrt{R}\exp(-i\omega_0\tau)Y_2(l,t-\tau) \tag{15}$$

In deriving Eq. (15) we neglected diffraction in the external cavity by implicitly assuming a self-imaging configuration. As anticipated in the introduction, although all the results reported

#156317 - $15.00 USD Received 11 Oct 2011; revised 9 Dec 2011; accepted 2 Jan 2012; published 5 Mar 2012

in this paper refer to this simpler case, our model accounts for non self-imaging cavity if Eq. (15) is replaced with:

$$\begin{aligned} Y_2(l,t) &= \varepsilon\sqrt{R_{ext}}\sqrt{1-R}\exp(-i\omega_0\tau)\sum_{p,m}E_{p,m}(t-\tau)\mathscr{D}A_{p,m} \\ &- \varepsilon\sqrt{R_{ext}}\sqrt{R}\exp(-i\omega_0\tau)\sum_{p,m}Y_{2,p,m}(l,t-\tau)\mathscr{D}A_{p,m} \end{aligned}$$

where $\mathscr{D}$ denotes the propagation operator of the Gauss-Laguerre functions $A_{p,m}$ in free space [43]. Clearly we get the self-imaging configuration when $\mathscr{D}$ is the identity operator. This for example allowed us to estimate the effect on the laser characteristics of a non perfect self-imaging, which is likely to occur experimentally.
Introducing relation (15) in Eq. (14) we obtain:

$$\begin{aligned} \frac{dE_{p,m}}{dt} &= \left(iq\Delta\omega_T - \frac{1}{2\tau_p}(1+i\alpha)\right)E_{p,m} + \frac{1}{2}G_n(1+i\alpha)\int_0^{2\pi}d\phi\int_0^{\infty}\rho d\rho A^*_{p,m}(N-N_0)E \\ &+ \frac{1}{\tau_c}\left(\varepsilon\frac{\sqrt{R_{ext}}(1-R)}{\sqrt{R}}\exp(-i\omega_0\tau)E_{p,m}(t-\tau) - \varepsilon\sqrt{R_{ext}}\sqrt{1-R}\exp(-i\omega_0\tau)Y_{p,m}(l,t-\tau)\right) \end{aligned} \quad (16)$$

where we put $Y_{2,p,m}(l,t-\tau) = Y_{p,m}(t-\tau)$. Finally, we may write in an alternative form Eq. (16):

$$\begin{aligned} \frac{dE_{p,m}(t)}{dt} &= \left(iq\Delta\omega_T - \frac{1}{2\tau_p}(1+i\alpha)\right)E_{p,m}(t) + \frac{1}{2}G_n(1+i\alpha)\int_0^{2\pi}d\phi\int_0^{\infty}\rho d\rho A^*_{p,m}(N(\rho,\phi,t)-N_0)E(\rho,\phi,t) \\ &+ \frac{1}{\tau_c}\left(\sum_{s=1}^{\infty}k_sE_{p,m}(t-s\tau)\exp(-is\omega_0\tau)\right) \end{aligned} \quad (17)$$

where the feedback coefficients k_s are given by:

$$k_s = \varepsilon^s\frac{(1-R)\sqrt{R_{ext}}}{\sqrt{R}}\left(-\sqrt{R}\sqrt{R_{ext}}\right)^{s-1}, \quad s\in\mathscr{N}$$

From Eq. (16) we derive Eq. (6) by further assuming a spatially modulated target and a single reflection in the external cavity.

Acknowledgments

We acknowledge partial financial support from Regione Puglia – Project *DM*01.1 related to the Apulian Technological District on Mechatronics (MEDIS) and MIUR – Project *PON*01_02238.
Lorenzo Columbo and Massimo Brambilla also acknowledge the Progetto FIRB – PROGRAMMA "FUTURO IN RICERCA" Anno 2008 – Protocollo: *RBFR*08*E*7*VA*_001.

#156317 - $15.00 USD Received 11 Oct 2011; revised 9 Dec 2011; accepted 2 Jan 2012; published 5 Mar 2012